Supporting Information

Theory-Guided Synthesis of Highly Luminescent Colloidal Cesium Tin Halide Perovskite Nanocrystals

Qi Liu,[†,¶] Jun Yin,[‡,¶] Bin-Bin Zhang,[§,//,¶] Jia-Kai Chen,[§,//] Yang Zhou,[‡] Lu-Min Zhang,[†] Lu-Ming Wang,[†] Qing Zhao,[§] Jingshan Hou,[⊥] Jie Shu,[#] Bo Song,[†] Naoto Shirahata,[§,//,△] Osman M. Bakr,[‡] Omar F. Mohammed,[*,‡] and Hong-Tao Sun[*,§]

[†]College of Chemistry, Chemical Engineering and Materials Science, Soochow University, Suzhou 215123, China

[‡]Advanced Membranes and Porous Materials Center (AMPMC) & KAUST Catalysis Center (KCC), Division of Physical Sciences and Engineering, King Abdullah University of Science and Technology (KAUST), Thuwal 23955-6900, Kingdom of Saudi Arabia

[§]International Center for Materials Nanoarchitectonics (MANA), National Institute for Materials Science (NIMS), 1-2-1 Sengen, Tsukuba 305-0047, Japan

[//] Graduate School of Chemical Sciences and Engineering, Hokkaido University, Sapporo 060-0814, Japan

[⊥] School of Materials Science and Engineering, Shanghai Institute of Technology, Shanghai 201418, China

[#]Analysis and Testing Center, Soochow University, Jiangsu 215123, China

[△]Department of Physics, Chuo University, Tokyo 112-8551, Japan

[¶]Q. Liu, J. Yin, and B.-B. Zhang contributed equally to this work.

Detailed method for the calculation of the average lifetime, radiative and non-radiative recombination rates: We used the following method to roughly evaluate the radiative and nonradiative recombination rates. The photoluminescence quantum yield (PLQY) is defined as the ratio of emitted photons per absorbed photons. The radiative recombination and the non-radiative recombination both depopulated the excited state. Hence, the PLQY is also defined as the ratio of the radiative recombination rate to the total recombination rate, given by equation (1),

$$PLQY = \frac{\Gamma_{rad}}{\Gamma_{rad} + \Gamma_{non-rad}} \quad (1)$$

where Γ_{rad} and $\Gamma_{non-rad}$ are the radiative and non-radiative recombination rates, respectively.

The lifetime of the excited state refers to the average residence time of the photon in the excited state before returning to the ground state. The average lifetime is the reciprocal of the total recombination rate, which is calculated using the following equation,

$$\tau_{ave} = \frac{1}{\Gamma_{rad} + \Gamma_{non-rad}} \quad (2)$$

where τ_{ave} is the average lifetime. The decays of $CsSnI_3$ NCs were fitted by a single-, bi- or tri-exponential function,

$$I(t) = A_1 e^{-t/\tau_1} + A_2 e^{-t/\tau_2} + A_3 e^{-t/\tau_3} + \cdots A_0 \quad (3)$$

where A_i (i=1, 2, and 3) and τ_i (i=1, 2, and 3) are the amplitudes and the corresponding fitted lifetimes, respectively, A_0 is a constant. The average lifetime (τ_{ave}) was calculated as follows,

$$\tau_{ave} = (A_1\tau_1^2 + A_2\tau_2^2 + A_3\tau_3^2 + \cdots)/(A_1\tau_1 + A_2\tau_2 + A_3\tau_3 + \cdots) \quad (4)$$

Based on the PLQY and τ_{ave}, we calculated the radiative and non-radiative recombination rates as follows,

$$\Gamma_{rad} = \frac{\mathrm{PLQY}}{\tau_{ave}} \quad (5)$$

$$\Gamma_{non-rad} = \frac{1}{\tau_{ave}} - \Gamma_{rad} = \frac{1 - \mathrm{PLQY}}{\tau_{ave}} \quad (6)$$

Defect calculations at the HSE06+SOC level. The HSE06 including SOC was also used to calculate defect formation energies and defect charge-transition levels. The contribution of the Hartree-Fock exchange potential was set at 0.25, and the plane-wave basis set cutoff of the wavefunctions was set at 400 eV. In equilibrium growth conditions, the chemical potential μ_i should satisfy the following equations: $\mu_{Cs} + \mu_{Sn} + 3\mu_I = \Delta H$ ($CsSnI_3$) = -7.35 eV; $\mu_{Sn} + 2\mu_I < \Delta H$ (SnI_2) = -1.76 eV; $\mu_{Cs} + \mu_I < \Delta H$ (CsI) = -5.31 eV.

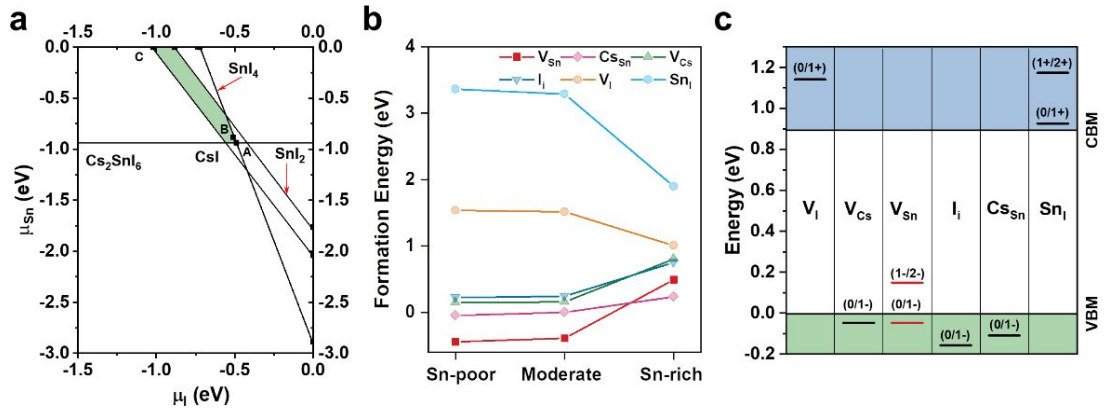

Figure S1. (a) Stability regions of different compounds vs. I and Sn chemical potentials of $CsSnI_3$. The shaded region indicates the equilibrium chemical potential region. The representative points (A: Sn-poor/I-rich, B: moderate, C: Sn-rich/I-poor conditions) are chosen for the defect formation energy calculations. (b) Calculated defect formation energies for 2×2×2 orthorhombic $CsSnI_3$ supercell at Sn-poor/I-rich, moderate, and Sn-rich/I-poor conditions, corresponding to A, B, C point in (a), respectively. (c) Defect charge-transition levels of $CsSnI_3$. These calculations were performed at the HSE06+SOC level of theory.

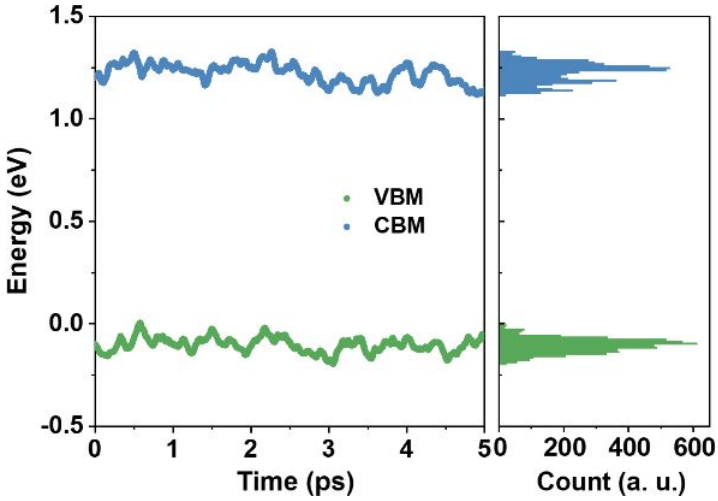

Figure S2. Time evolution of the VBM and CBM for 2×2×2 $CsSnI_3$ supercell with Cs_{Sn} at 300 K. The fluctuation widths of VBM and CBM for pristine $CsSnI_3$ are 0.200 and 0.209 eV, respectively.

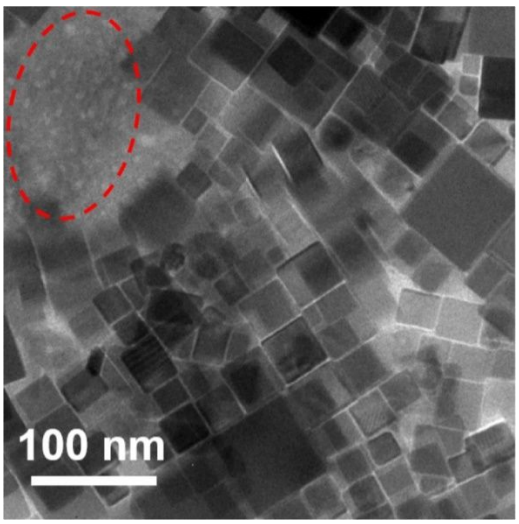

Figure S3. Low-magnification TEM image of 0.25:4.8. The area in the plotted ellipse indicates the presence of some byproducts.

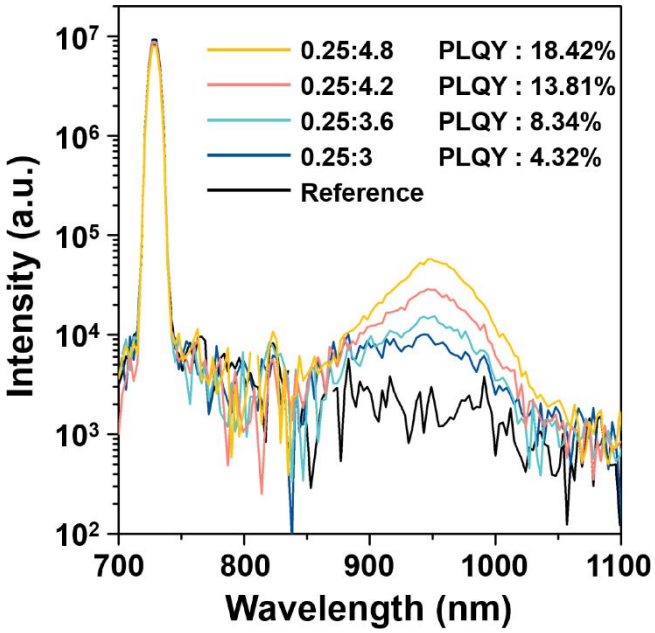

Figure S4. PLQY measurements of $CsSnI_3$ NCs prepared with different Cs:Sn precursor ratios.

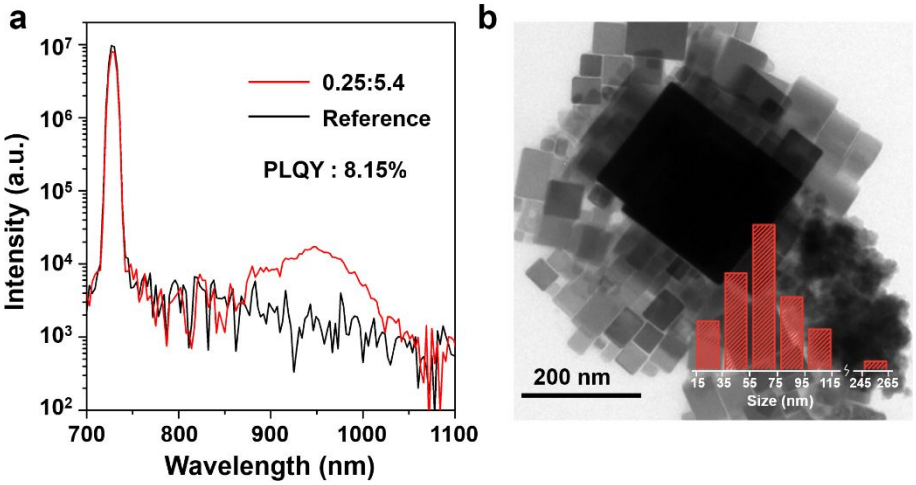

Figure S5. (a) PLQY measurement and (b) TEM image of 0.25:5.4. Inset in (b) shows the histogram of edge lengths of corresponding NCs.

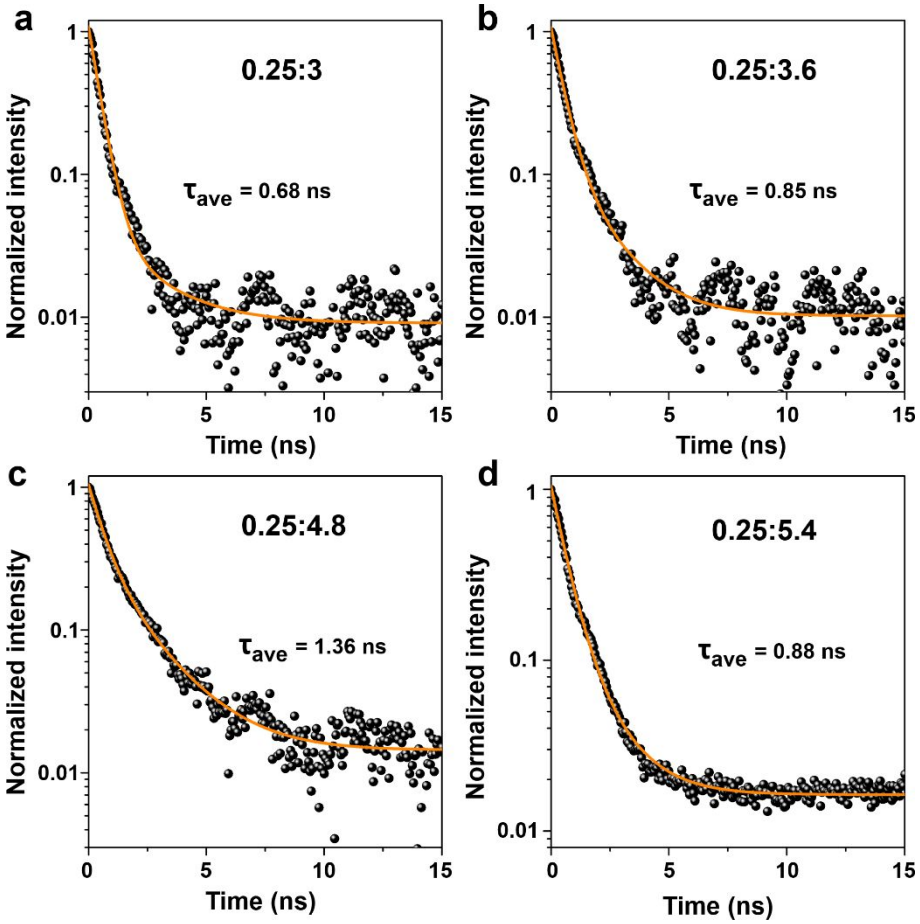

Figure S6. PL decays (black dots) and fitted curves (red lines) of (a) 0.25:3, (b) 0.25:3.6, (c) 0.25:4.8, and (d) 0.25:5.4 NCs.

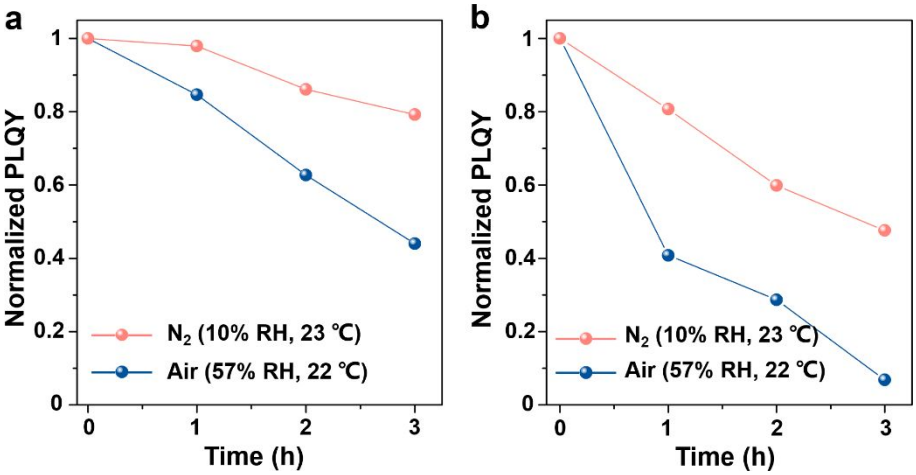

Figure S7. a) Temporal evolution of PLQYs of 0.25:4.2 NCs dispersed in hexane in air (57% relative humidity, RH) and under N_2 atmosphere (10% RH). For OAm and OA, their combination with NCs is highly dynamic and labile. This degradation can be linked to the low density of ligands on the surface. b) Temporal evolution of PLQYs of the $CsSnI_3$ NCs synthesized according to the reported strategy.[1]

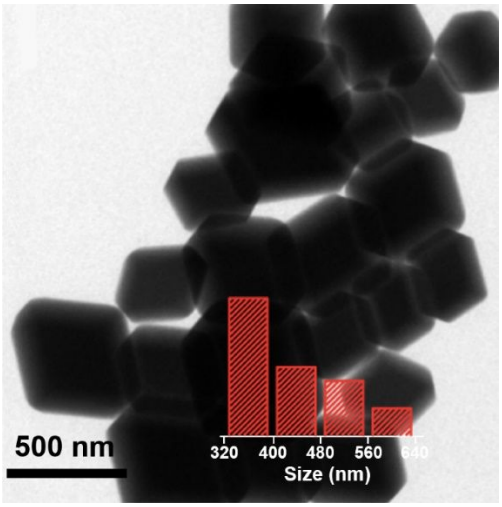

Figure S8. Low-magnification TEM image of 0.25:4.2:2 NCs. Inset shows the histogram of edge lengths of corresponding NCs.

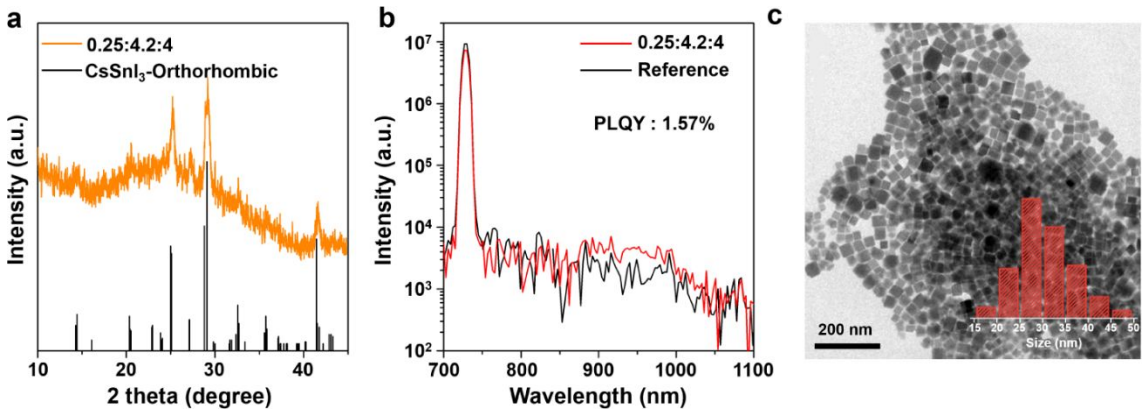

Figure S9. (a) XRD pattern of 0.25:4.2:4 NCs. (b) PLQY measurement and (c) TEM image of 0.25:4.2:4 NCs. Inset in (c) shows the histogram of edge lengths of corresponding NCs.

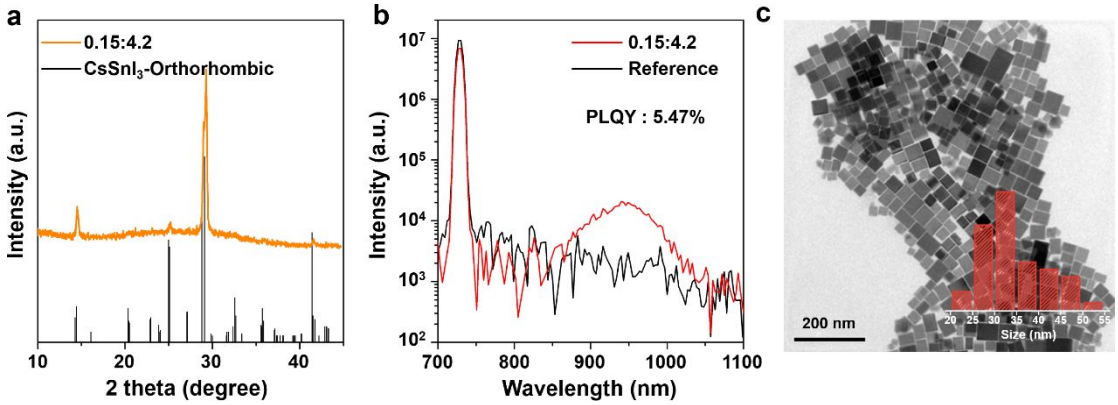

Figure S10. (a) XRD pattern of 0.15:4.2 NCs. (b) PLQY measurement and (c) TEM image of 0.15:4.2 NCs. Inset in (c) shows the histogram of edge lengths of corresponding NCs.

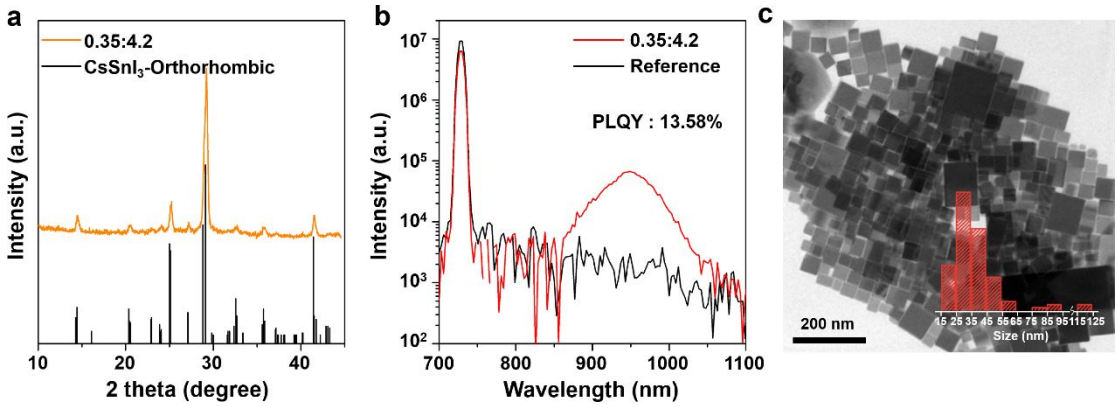

Figure S11. (a) XRD pattern of 0.35:4.2 NCs. (b) PLQY measurement and (c) TEM image of 0.35:4.2 NCs. Inset in (c) shows the histogram of edge lengths of corresponding NCs.

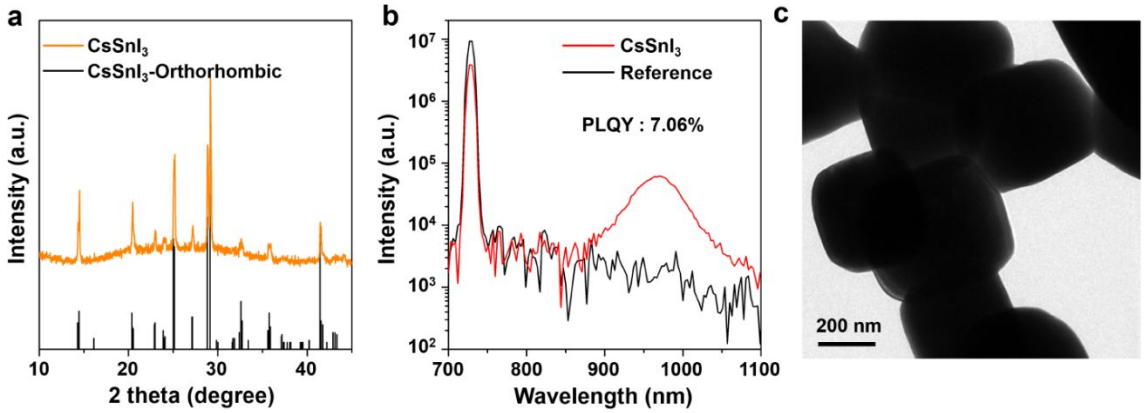

Figure S12. (a) XRD pattern, (b) PLQY measurement, and (c) TEM image of the product. $CsSnI_3$ was synthesized by replacing TMSI with equimolar amount of benzoyl iodine, while keeping the other synthetic parameters same with those of 0.25:4.2.

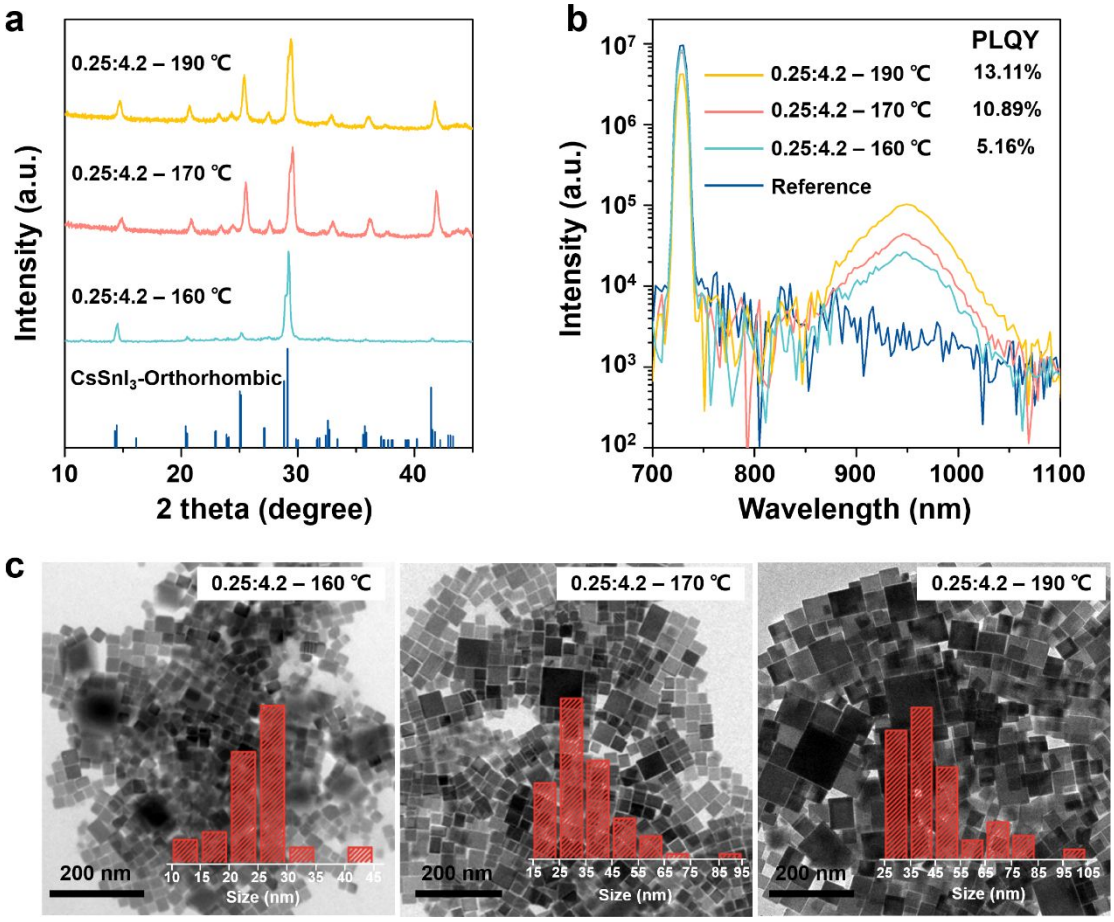

Figure S13. (a) XRD patterns, (b) PLQY measurement, and (c) TEM images of $CsSnI_3$ NCs synthesized at different temperatures. We note that the PLQYs and size of $CsSnI_3$ NCs increase with increasing reaction temperatures.

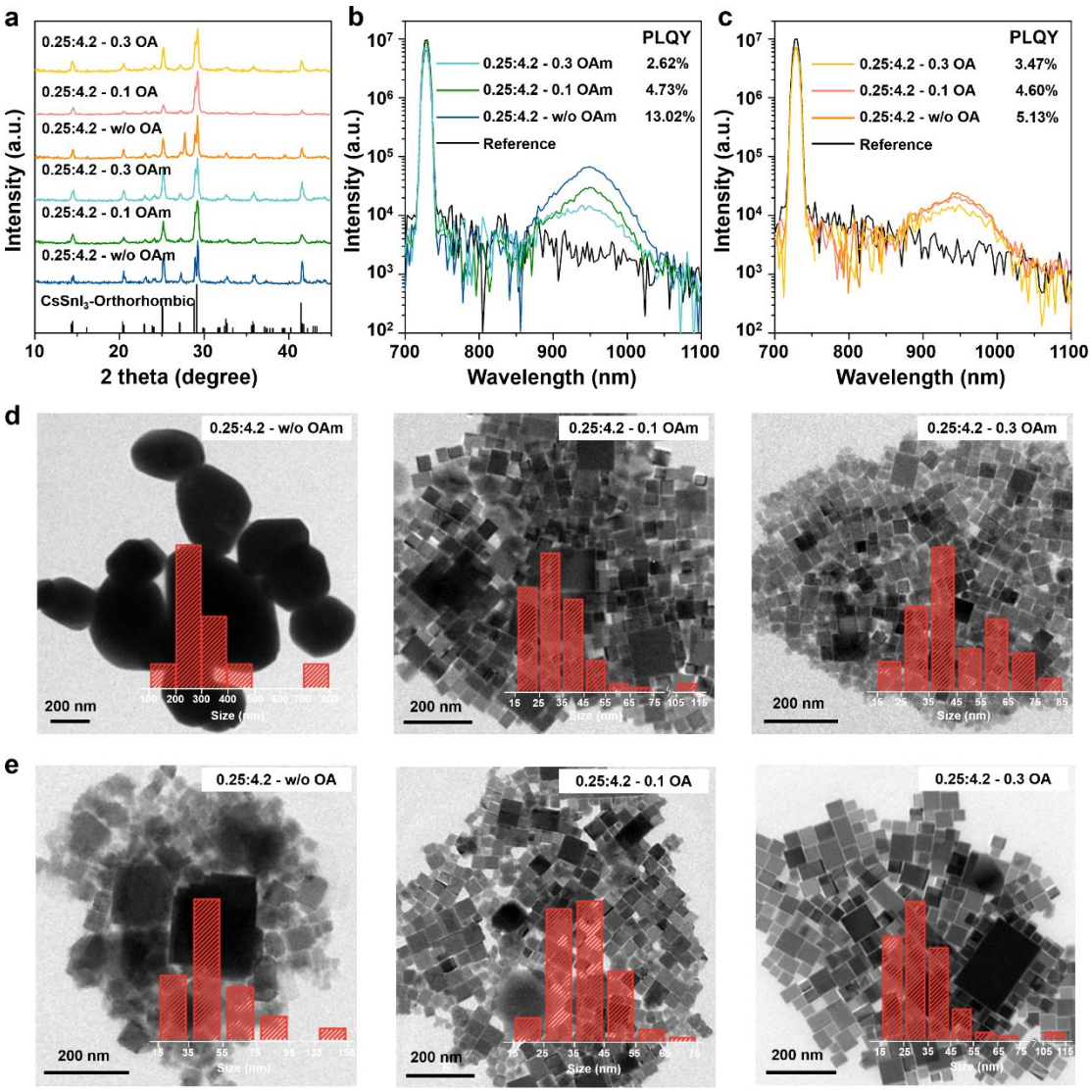

Figure S14. (a) XRD patterns, (b, c) PLQY measurement, and (d, e) TEM images of $CsSnI_3$ NCs synthesized with different amounts of OA and OAm. The detailed synthetic parameters are shown in Table S1. The final size of 0.25:4.2-w/o OAm exceeds 100 nm (Figure S14d, on the left), indicating that OAm plays a very important role in controlling the growth rate of $CsSnI_3$. The larger the size, the smaller the specific surface area. That is, less defects on the surface of NCs could contribute to the high PLQY.

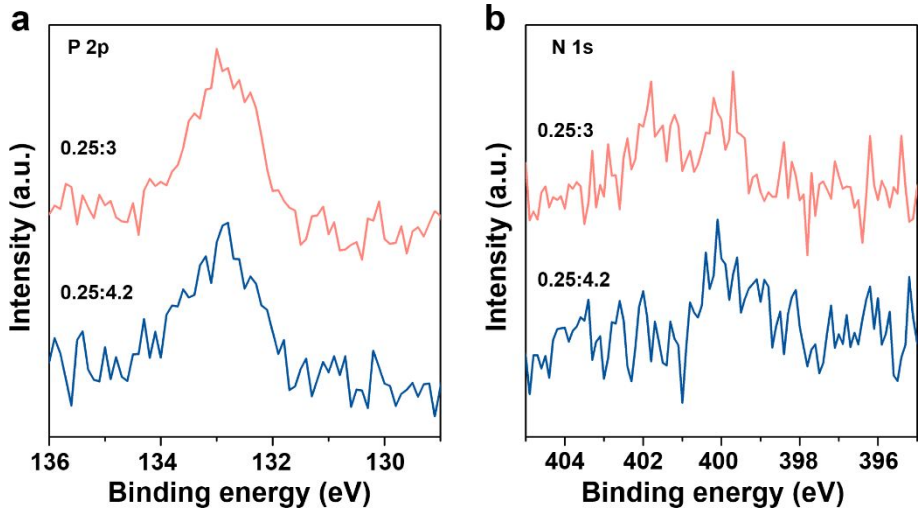

Figure S15. High-resolution XPS spectra of (a) P 2p and (b) N 1s for 0.25:3 and 0.25:4.2 NCs. The binding energies were calibrated using the free carbon C 1s peak at 284.8 eV.

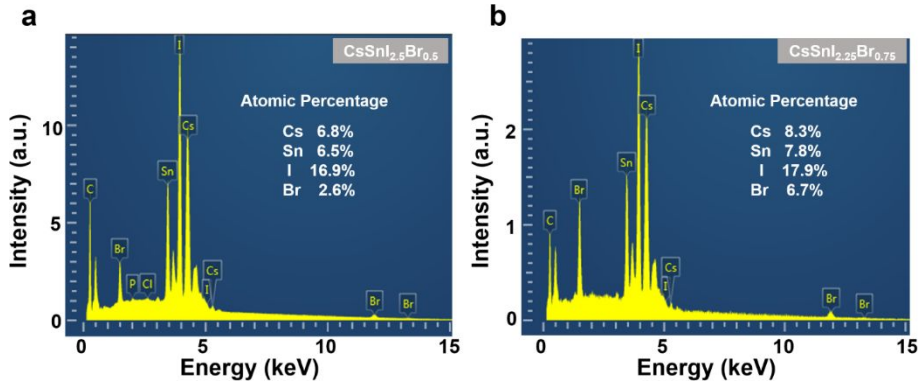

Figure S16. EDS of (a) $CsSnI_{2.5}Br_{0.5}$ and (b) $CsSnI_{2.25}Br_{0.75}$ NCs. Note that we used the nominal compositions for denoting the products.

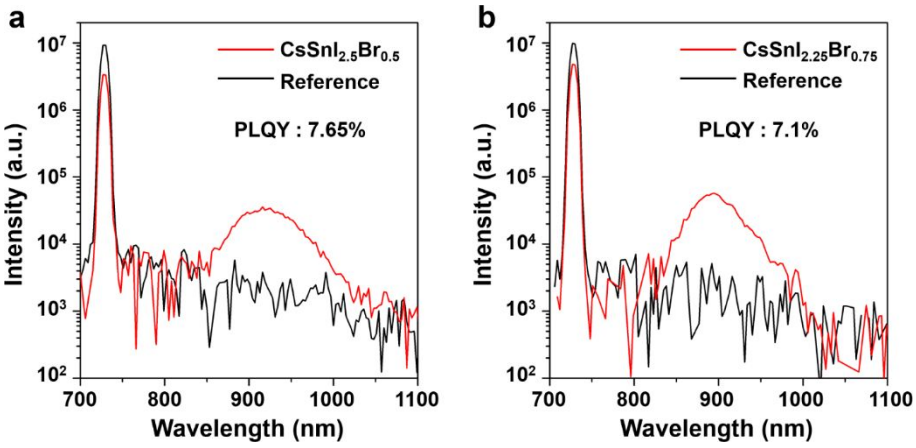

Figure S17. PLQY measurement of (a) $CsSnI_{2.5}Br_{0.5}$ and (b) $CsSnI_{2.25}Br_{0.75}$ NCs.

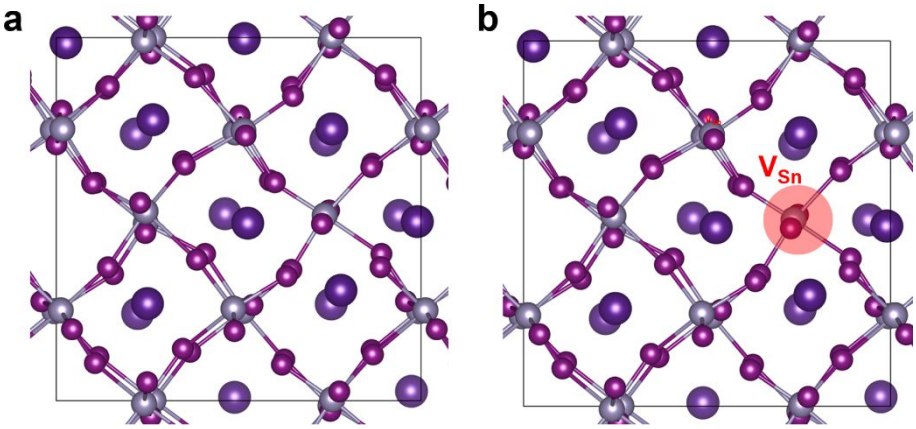

Figure S18. (a) 2×2×2 pristine $CsSnI_3$ and (b) $CsSnI_3$ supercell with V_{Sn} used for the MD simulations.

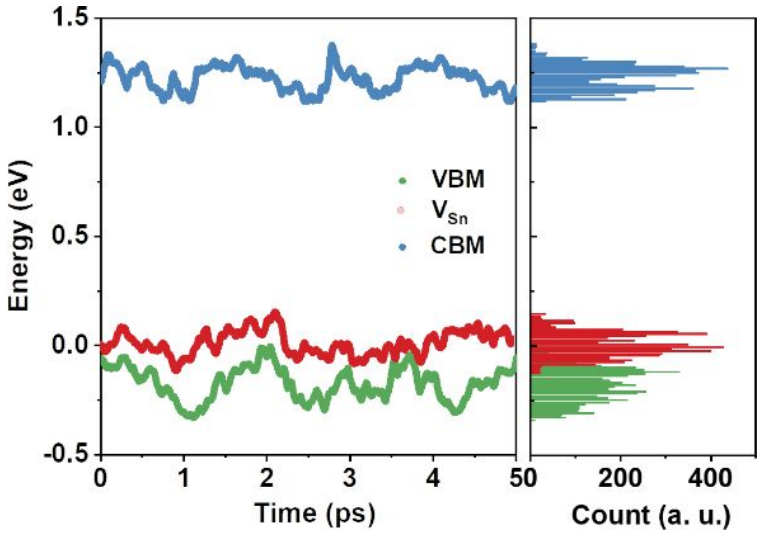

Figure S19. Time evolution of the VBM and CBM for 2×2×1 $CsSnI_3$ supercell with V_{Sn} at 300 K. The fluctuation widths of VBM and CBM are 0.327 and 0.257 eV, respectively.

Table S1. Synthetic parameters used for the synthesis of $CsSnI_3$, $CsSnI_{2.5}Br_{0.5}$, and $CsSnI_{2.25}Br_{0.75}$ NCs. We note that 0.25:4.2:2 and 0.25:4.2:4 NCs are denoted by the molar ratio of Cs, Sn and I precursors, while for the 0.25:4.2-*x* NCs, *x* represents either the reaction temperature or the parameter related to ligands. The exact amount of chemicals with purity less than 99.9% was calculated after considering their respective purity. For oleylamine, the purity of 85% was used for the calculation.

Sample	Cs_2CO_3 (g)	$Sn(Oct)_2$ (mL)	TMSI (mL)	TMSBr (mL)	OA (mL)	OAm (mL)	TOP (mL)	Temperature (°C)
0.25:3	0.0326	0.80	0.344	/	0.2	0.2	1.63	180
0.25:3.6	0.0326	0.96	0.344	/	0.2	0.2	1.63	180
0.25:4.2	0.0326	1.12	0.344	/	0.2	0.2	1.63	180
0.25:4.8	0.0326	1.28	0.344	/	0.2	0.2	1.63	180
0.25:5.4	0.0326	1.44	0.344	/	0.2	0.2	1.63	180
0.15:4.2	0.0196	1.12	0.344	/	0.2	0.2	1.63	180
0.35:4.2	0.0456	1.12	0.344	/	0.2	0.2	1.63	180
0.25:4.2:2	0.0326	1.12	0.229	/	0.2	0.2	1.63	180
0.25:4.2:4	0.0326	1.12	0.458	/	0.2	0.2	1.63	180
0.25:4.2-160 ℃	0.0326	1.12	0.344	/	0.2	0.2	1.63	160
0.25:4.2-170 ℃	0.0326	1.12	0.344	/	0.2	0.2	1.63	170
0.25:4.2-190 ℃	0.0326	1.12	0.344	/	0.2	0.2	1.63	190
0.25:4.2-w/o OAm	0.0326	1.12	0.344	/	0.2	/	1.63	180
0.25:4.2-0.1 OAm	0.0326	1.12	0.344	/	0.2	0.1	1.63	180
0.25:4.2-0.3 OAm	0.0326	1.12	0.344	/	0.2	0.3	1.63	180
0.25:4.2-w/o OA	0.0326	1.12	0.344	/	/	0.2	1.63	180
0.25:4.2-0.1 OA	0.0326	1.12	0.344	/	0.1	0.2	1.63	180
0.25:4.2- 0.3 OA	0.0326	1.12	0.344	/	0.3	0.2	1.63	180
$CsSnI_{2.5}Br_{0.5}$	0.0326	1.12	0.287	0.053	0.2	0.2	1.63	180
$CsSnI_{2.25}Br_{0.75}$	0.0326	1.12	0.259	0.080	0.2	0.2	1.63	180

Table S2. Summary of the average NC's size and distribution, PL fwhm, PLQY, and average lifetimes (τ_{ave}) for typical samples.

Sample	PLQY (%)	PL FWHM (nm)	Average NC's size (nm)	Size distribution (nm)	τ_{ave} (ns)
0.25:3	4.3	93	26	15-45	0.70
0.25:3.6	8.3	81	29	15-45	0.85
0.25:4.2	13.8	77	33	20-45	1.26
0.25:4.8	18.4	79	37	10-170	1.36
0.25:5.4	8.2	80	63	15-265	0.88

Table S3. Fitting results of PL decay curves, τ_{ave}, PLQYs, radiative (Γ_{rad}) and nonradiative ($\Gamma_{non\text{-}rad}$) decay rates of $CsSnI_3$ and $CsSn(I, Br)_3$ NCs. Note that only the decay curve of 0.25:3 was fitted by a tri-exponential function, because it cannot be fitted well by a double-exponential function. It is also necessary to fit the decays of 0.25:3.6, 0.25:4.2 and 0.25:4.8 by a double-exponential function.

Sample	A_1	τ_1 (ns)	A_2	τ_2 (ns)	A_3	τ_3 (ns)	A_0	Adjusted R-square	τ_{ave} (ns)	PLQY (%)	Γ_{rad} (μs^{-1})	$\Gamma_{non\text{-}rad}$ (μs^{-1})
0.25:3	0.54	0.42	0.50	0.42	0.04	2.13	0.0091	0.9940	0.70	4.3	61.43	1367.14
0.25:3.6	0.93	0.48	0.13	1.63			0.0102	0.9959	0.85	8.3	97.65	1078.82
0.25:4.2	1.00	0.69	0.07	3.07			0.0141	0.9952	1.26	13.8	109.52	684.41
0.25:4.8	0.74	0.61	0.29	1.95			0.0144	0.9977	1.36	18.4	135.29	600.00
0.25:5.4	0.86	0.58	0.17	1.49			0.0163	0.9970	0.88	8.2	93.18	1043.18
$CsSnI_{2.5}Br_{0.5}$	0.85	0.56	0.09	3.84			0.0835	0.9927	1.94	7.7	39.69	475.77
$CsSnI_{2.25}Br_{0.75}$	1.03	1.67					0.0251	0.9928	1.67	7.1	42.51	556.29

Table S4. IR vibrational modes and their assignments for $CsSnI_3$ NCs.

Frequency (cm^{-1})	Functional group assigned	References
2926	C-H stretching vibration of methylene group (CH_2)	2
2854	C-H stretching vibration of methyl group (CH_3)	2
1745	C=O stretching vibration	2
1649	C=C stretching vibration	3
1541	COO- asymmetric stretching vibration	2,4
1462	C-H bending vibration of methylene group (CH_2)	5
1377	C-H bending vibration of methyl group (CH_3)	6
1082	C-P stretching vibration	7,8
721	C-H out-of-plane vibration or C-C stretching vibrations	9-11

Table S5. Summary of ligand density of perovskite NCs solutions.

Sample	Ligand	Ligand density (nm^{-2})	References
$CsPbCl_3$	OA + OAm	25.31	4
$CsPbBr_3$[a]	OA + OAm	6.7	12
$CsPbI_3$	OA + OAm	25-40	3
$FAPbI_3$	OA + OAm	20-35	3
$CsSnI_3$	OA + OAm	1.8	This work
	TOP	2.0	

[a] The sample used for the characterization is the product of as-synthesized NCs that undergo one-cycle ligand removal.

REFERENCES

(1) Jellicoe, T. C.; Richter, J. M.; Glass, H. F. J.; Tabachnyk, M.; Brady, R.; Dutton, S. E.; Rao, A.; Friend, R. H.; Credgington, D.; Greenham, N. C.; Böhm, M. L. Synthesis and Optical Properties of Lead-Free Cesium Tin Halide Perovskite Nanocrystals. *J. Am. Chem. Soc.* **2016**, *138* (9), 2941-2944.

(2) Chiba, T.; Hayashi, Y.; Ebe, H.; Hoshi, K.; Sato, J.; Sato, S.; Pu, Y.-J.; Ohisa, S.; Kido, J. Anion-exchange red perovskite quantum dots with ammonium iodine salts for highly efficient light-emitting devices. *Nat. Photonics* **2018**, *12* (11), 681-687.

(3) Hao, M.; Bai, Y.; Zeiske, S.; Ren, L.; Liu, J.; Yuan, Y.; Zarrabi, N.; Cheng, N.; Ghasemi, M.; Chen, P.; Lyu, M.; He, D.; Yun, J.-H.; Du, Y.; Wang, Y.; Ding, S.; Armin, A.; Meredith, P.; Liu, G.; Cheng, H.-M.; Wang, L. Ligand-assisted cation-exchange engineering for high-efficiency colloidal $Cs_{1-x}FA_xPbI3$ quantum dot solar cells with reduced phase segregation. *Nat. Energy* **2020**, *5* (1), 79-88.

(4) Shen, X.; Zhang, Y.; Kershaw, S. V.; Li, T.; Wang, C.; Zhang, X.; Wang, W.; Li, D.; Wang, Y.; Lu, M.; Zhang, L.; Sun, C.; Zhao, D.; Qin, G.; Bai, X.; Yu, W. W.; Rogach, A. L. Zn-Alloyed $CsPbI_3$ Nanocrystals for Highly Efficient Perovskite Light-Emitting Devices. *Nano Lett.* **2019**, *19* (3), 1552-1559.

(5) Pan, J.; Quan, L. N.; Zhao, Y.; Peng, W.; Murali, B.; Sarmah, S. P.; Yuan, M.; Sinatra, L.; Alyami, N. M.; Liu, J.; et al. Highly Efficient Perovskite-Quantum-Dot Light-Emitting Diodes by Surface Engineering. *Adv. Mater.* **2016**, *28* (39), 8718-8725.

(6) Arief, V. O.; Trilestari, K.; Sunarso, J.; Indraswati, N.; Ismadji, S. Recent Progress on Biosorption of Heavy Metals from Liquids Using Low Cost Biosorbents: Characterization, Biosorption Parameters and Mechanism Studies. *CLEAN - Soil, Air, Water* **2008,** *36* (12), 937-962.

(7) Chen, S.; Zhang, X.; Zhang, Q.; Tan, W. Trioctylphosphine as Both Solvent and Stabilizer to Synthesize CdS Nanorods. *Nanoscale Res. Lett.* **2009,** *4* (10), 1159-1165.

(8) Liu, F.; Zhang, Y.; Ding, C.; Kobayashi, S.; Izuishi, T.; Nakazawa, N.; Toyoda, T.; Ohta, T.; Hayase, S.; Minemoto, T.; Yoshino, K.; Dai, S.; Shen, Q. Highly Luminescent Phase-Stable $CsPbI_3$ Perovskite Quantum Dots Achieving Near 100% Absolute Photoluminescence Quantum Yield. *ACS Nano* **2017,** *11* (10), 10373-10383.

(9) Mourdikoudis, S.; Liz-Marzán, L. M. Oleylamine in Nanoparticle Synthesis. *Chem. Mater.* **2013,** *25* (9), 1465-1476.

(10) Sinclair, R. G.; McKay, A. F.; Jones, R. N. The Infrared Absorption Spectra of Saturated Fatty Acids and Esters[1]. *J. Am. Chem. Soc.* **1952,** *74* (10), 2570-2575.

(11) Pan, J.; Shang, Y.; Yin, J.; De Bastiani, M.; Peng, W.; Dursun, I.; Sinatra, L.; El-Zohry, A. M.; Hedhili, M. N.; Emwas, A. H.; Mohammed, O. F.; Ning, Z.; Bakr, O. M., Bidentate Ligand-Passivated $CsPbI_3$ Perovskite Nanocrystals for Stable Near-Unity Photoluminescence Quantum Yield and Efficient Red Light-Emitting Diodes. *J. Am. Chem. Soc.* **2018,** *140* (2), 562-565.

(12) Li, J.; Xu, L.; Wang, T.; Song, J.; Chen, J.; Xue, J.; Dong, Y.; Cai, B.; Shan, Q.; Han, B.; et al. 50-Fold EQE improvement up to 6.27% of solution-processed all-inorganic perovskite $CsPbBr_3$ QLEDs via surface ligand density control. *Adv. Mater.* **2017**, *29* (5), 1603885.